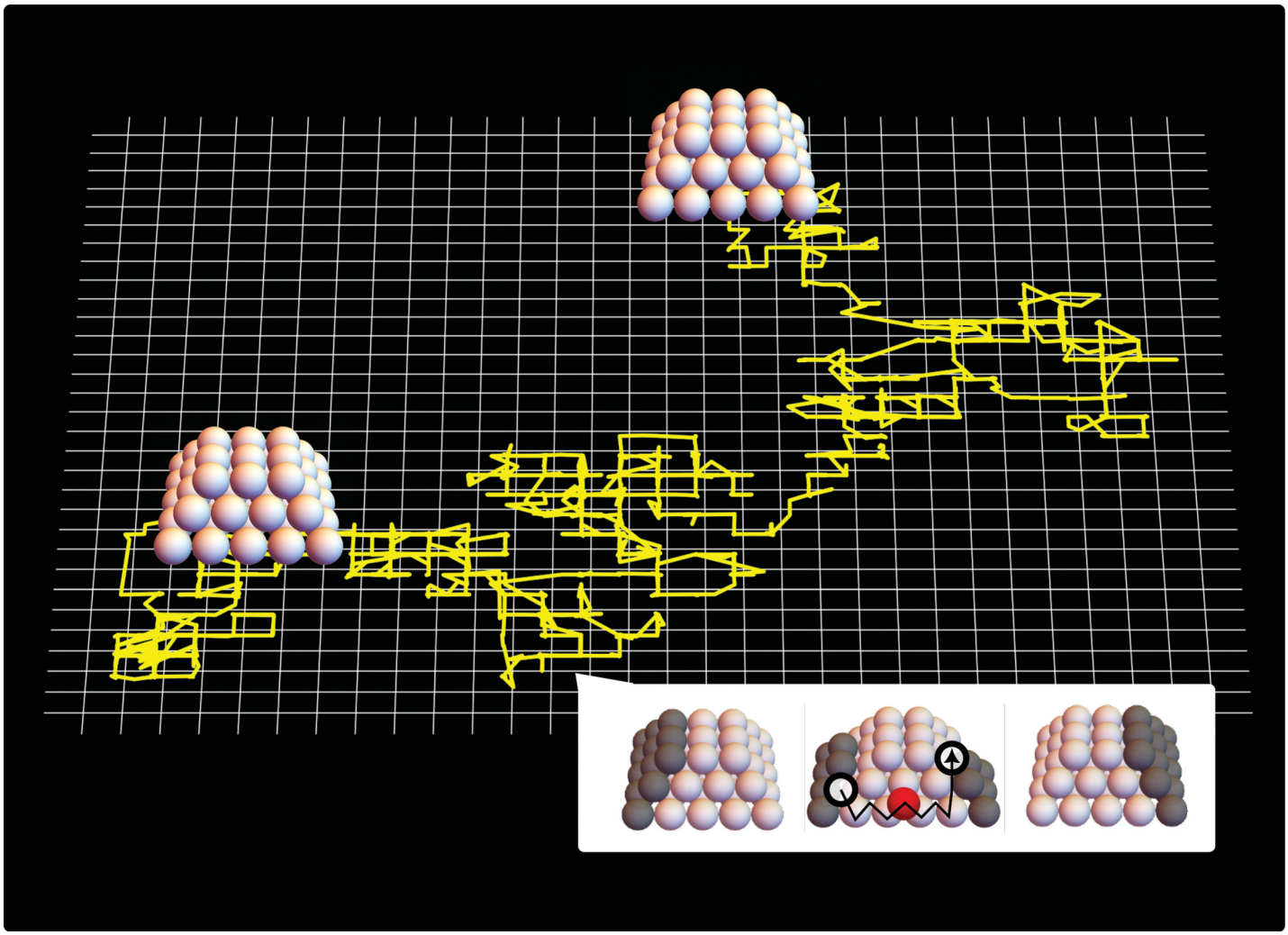

Showcasing research from the group of Professor Jim Evans at Ames National Laboratory USDOE and Iowa State University, USA, in collaboration with Professor Charlie Campbell at the University of Washington, USA.

Size-dependent diffusion of supported metal nanoclusters: mean-field-type treatments and beyond for faceted clusters

Diffusion of facetted epitaxially-supported nanoclusters is not described by the standard mean-field picture of random independent hopping of surface atoms. Instead, a cooperative many-atom mechanism is operative involving disassembly and reassembly of outer layers of facets. The latter results in strong oscillations in diffusivity versus nanocluster size, minima corresponding to closed-shell sizes. The effective barrier for the cooperative process is far higher than the mean-field prediction.

As featured in:

See James W. Evans *et al.*, *Nanoscale Horiz.*, 2023, **8**, 1556.

ROYAL SOCIETY OF CHEMISTRY

rsc.li/nanoscale-horizons

Registered charity number: 207890

Nanoscale Horizons

ROYAL SOCIETY OF CHEMISTRY

COMMUNICATION

View Article Online
View Journal | View Issue

Cite this: *Nanoscale Horiz.*, 2023, **8**, 1556

Received 14th April 2023,
Accepted 31st July 2023

DOI: 10.1039/d3nh00140g

rsc.li/nanoscale-horizons

Size-dependent diffusion of supported metal nanoclusters: mean-field-type treatments and beyond for faceted clusters†

King C. Lai, ‡[ab] Charles T. Campbell [c] and James W. Evans *[ab]

Nanostructured systems are intrinsically metastable and subject to coarsening. For supported 3D metal nanoclusters (NCs), coarsening can involve NC diffusion across the support and subsequent coalescence (as an alternative to Ostwald ripening). When used as catalysts, this leads to deactivation. The dependence of diffusivity, D_N, on NC size, N (in atoms), controls coarsening kinetics. Traditional mean-field (MF) theory for D_N *versus* N assumes that NC diffusion is mediated by independent random hopping of surface adatoms with low coordination, and predicts that $D_N \sim hN^{-4/3}n_{eq}$. Here, $h = \nu\exp[-E_d/(k_BT)]$ denotes the hop rate, and $n_{eq} = \exp[-E_{form}/(k_BT)]$ the density of those adatoms. The adatom formation energy, E_{form}, approaches a finite large-N limit, as does the effective barrier, $E_{eff} = E_d + E_{form}$, for NC diffusion. This MF theory is critically assessed for a realistic stochastic atomistic model for diffusion of faceted fcc metal NCs with a {100} facet epitaxially attached to a (100) support surface. First, the MF formulation is refined to account for distinct densities and hop rates for surface adatoms on different facets and along the base contact line, and to incorporate the exact values of E_{form} and n_{eq} *versus* N for our model. MF theory then captures the occurrence of local minima in D_N *versus* N at closed-shell sizes, as shown by KMC simulation. However, the MF treatment also displays fundamental shortcomings due to the feature that diffusion of faceted NCs is actually dominated by a cooperative multi-step process involving disassembling and reforming of outer layers on side facets. This mechanism leads to an E_{eff} which is well above MF values, and which increases with N, features captured by a beyond-MF treatment.

New concepts

Diverse nanostructured materials are increasingly utilized for energy and environmental technologies including catalysis. However, these systems are generally intrinsically metastable and are subject to coarsening. A key challenge is to elucidate coarsening pathways and to characterize kinetics. A prominent example is supported 3D metal nanoclusters (NCs) which can coarsen either *via* Ostwald ripening (OR) or *via* particle migration and coalescence (PMC). For PMC, coarsening kinetics is determined entirely by the size-dependence of NC diffusivity. However, only mean-field (MF) treatments of this dependence have been generally available and utilized, where NC motion is assumed to derive from independent random hopping of surface adatoms. Our analysis shows that this assumption is incorrect for faceted epitaxially-supported NCs, and that an alternative conceptual framework is needed to describe NC diffusion. We show that accounting for the appropriate cooperative multi-step mechanism underlying NC diffusion does capture the size-dependence of NC diffusion coefficients and of the associated activation energies.

Introduction

Coarsening in nanostructured bulk and surface systems has long been of interest[1,2] since such structure evolution generally impacts system properties. A common mechanism is Ostwald ripening (OR) discovered in the late 19th century,[3] for which appropriate LSW theory was developed in the mid-20th century.[4,5] For systems of supported 3D metal nanoclusters (NCs), rather than OR wherein metal monomers diffuse from smaller to larger NCs, coarsening can instead be mediated by particle (*i.e.*, NC) migration and coalescence (PMC).[6–14] PMC is sometimes also described as Smoluchowski ripening (SR), as opposed to OR. Coarsening *via* SR (as well as OR) is of particular importance with regard to deactivation for catalysts involving supported nanoparticles.[6–14] The kinetics of coarsening *via* PMC is determined entirely by the size-dependence of the diffusion coefficient for supported NCs.[6,15] Consequently, reliable treatment of PMC kinetics requires a predictive theoretical description of NC diffusivity.

[a] *Division of Chemical & Biological Sciences, Ames National Laboratory – USDOE, Ames, Iowa 50011, USA. E-mail: evans@ameslab.gov*
[b] *Department of Physics & Astronomy, Iowa State University, Ames, Iowa 50011, USA*
[c] *Chemistry Department, University of Washington, Seattle, Washington 98195, USA*

† Electronic supplementary information (ESI) available. See DOI: https://doi.org/10.1039/d3nh00140g

‡ Current address: Fritz Haber Institut der Max Planck Gesellschaft, 14195 Berlin, Germany.

The standard treatment of the diffusivity of supported 3D NCs is based on a mean-field (MF) picture wherein lateral motion of the center of mass of an NC of N atoms is associated with essentially random independent hopping of mobile surface adatoms across the NC surface.[6,16–19] In this treatment, such adatom diffusion is described by a single characteristic hop rate $h = \nu \exp[-\beta E_d]$. Here, E_d denotes the diffusion barrier, ν is the attempt frequency, and $\beta = (k_B T)^{-1}$ denotes the inverse temperature (where k_B is the Boltzmann constant, T is the surface temperature). In this scenario, each hop of a surface atom shifts the NC center of mass (CM) laterally by $\delta R_{CM} \sim a/N$, where 'a' is the surface lattice constant. The NC surface area, A (in units of adsorption sites) scales like $A \sim N^{2/3}$, and the total rate of surface atom hopping scales like $H \sim hAn_{eq}$, where $n_{eq} = \exp[-\beta E_{form}(N)]$ is the density (the number per adsorption site) of mobile surface adatoms. Here, E_{form} is the adatom formation energy which together with n_{eq} depends on NC size as typically determined by continuum Gibbs–Thompson (GT) type relations.[11,20] As an aside, natural extensions of GT relations can be developed for small faceted NCs (see the ESI†). The MF treatment predicts that the NC diffusion coefficient satisfies

$$D_N \sim H(\delta R_{CM})^2 \sim \nu a^2 N^{-4/3} \exp[-\beta E_{eff}(N)], \quad \text{where } E_{eff}(N) = E_d + E_{form}(N). \tag{1}$$

As $N \to \infty$, $E_{form}(N)$ approaches a finite value reflecting bulk and surface thermo-dynamics. Note that $N^{-4/3}$ size-scaling was also predicted for bulk diffusion of 3D voids.[21]

In the following, we first describe the atomistic-level stochastic model on which we base our analysis of the diffusion of {100} epitaxially-supported faceted fcc metal NCs. Next, a refinement of the conventional MF-treatment of NC diffusion is provided which is appropriate for faceted NCs considered here. Then, we present results from our refined MF analysis for NC diffusivity *versus* NC size, N, and compare these with accurate benchmark results previously obtained for the stochastic model from Kinetic Monte Carlo (KMC) simulation. Finally, we describe and present results from an appropriate beyond-MF formulation accounting for the feature that diffusion of faceted NCs is actually mediated by a cooperative multi-step process, rather than MF-type independent random hopping of NC surface atoms. Specifically, the multi-step process involves disassembly and reformation of outer layers on the side facets of the NC. Finally, conclusions are provided.

Stochastic atomistic model for {100}-epitaxial fcc metal nanoclusters

We utilize a stochastic lattice-gas model for {100} epitaxially-supported fcc metal NCs where the (potential) energy of the system is modeled by an effective nearest-neighbor (NN) pairwise attraction of strength $\phi > 0$ between metal atoms.[22] The effectiveness of this prescription of energetics is validated by DFT analysis,[23] and by extensive previous modeling of homoepitaxial growth and relaxation of thin metal films.[24,25] Note that ϕ is chosen to recover surface thermodynamics, and is well below one sixth of the bulk cohesive energy, E_c, which would recover bulk thermodynamics. The model applies for any fcc metal. However, we will perform simulations here with parameters corresponding to Ag, choosing $\phi = 0.225$ eV *versus* $E_c/6 = 0.49$ eV.[12] For {100}-epitaxially supported clusters, we regard each atom in the lowest {100} layer of the metal NC as interacting with each of four atoms in a top {100} layer of the support with an attraction of strength $f\phi$. Thus, $f > 0$ measures the strength of adhesion with $f = 1$ corresponding to fcc{100} homoepitaxy. The modeling in this paper will neglect possible vibrational entropy differences between various NC structures (but in some cases consider configurational entropy differences).

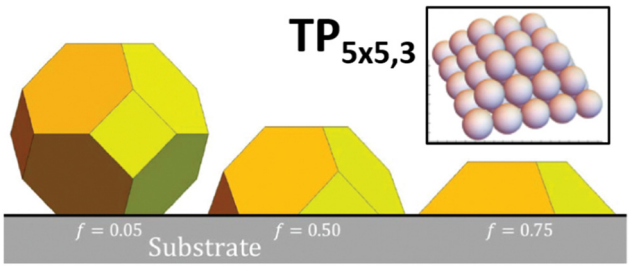

Fig. 1 Winterbottom shapes of supported clusters for a fcc metal. We consider the case with substantial adhesion $f = 0.75$.

For this fcc lattice-gas model with NN interactions, the large-size continuum equilibrium Wulff shape for unsupported NCs is a truncated octahedron with all edges between {100} and {111} facets of equal length.[26] The large-size continuum equilibrium Winterbottom shape for supported NCs truncates a portion of the Wulff NC dependent on the value of f. See Fig. 1.

To facilitate detailed atomistic-level analysis, we consider the case of strong adhesion, $f = 0.75$, where the continuum Winterbottom shape is a simple truncated pyramid (TP) with all edges having equal length.[22] In the atomistic model, for general discrete NC sizes, N (in atoms), the most stable ground state shape will not be a perfect truncated pyramid. However, one might anticipate the existence of a sequence of closed-shell sizes, N_{cs}, corresponding to perfect TPs which constitute non-degenerate ground states configurations. This is the case. Such clusters with an $n \times m$ atom base (where $m = n$ or $n \pm 1$) which are k layers tall will be denoted by $TP_{n\times m,k}$.

A comprehensive analysis of ground state NC configurations and energetics (as well as their configurational degeneracy) for the lattice-gas model with $f = 0.75$ was performed for NC sizes $N = 13$–126. Extensive results are provided in the ESI.† However, an illustrative portion of these results is presented in Fig. 2 showing schematics of non-perfect TP ground state configurations between two particularly stable magic closed-shell sizes $N_{cs} = 50$ ($TP_{5\times5,3}$) and $N_{cs} = 62$ ($TP_{5\times6,3}$) with perfect TP configurations, and in Table 1 which tabulates for ground state energies and configurational degeneracies for $N = 50$–65. These magic sizes, which correspond to deep local minima in D_N, are highlighted in bold italic font in Table 1. For non-closed shell sizes, we note that ground state degeneracy occurs in a significant fraction of cases as indicated by listing the various

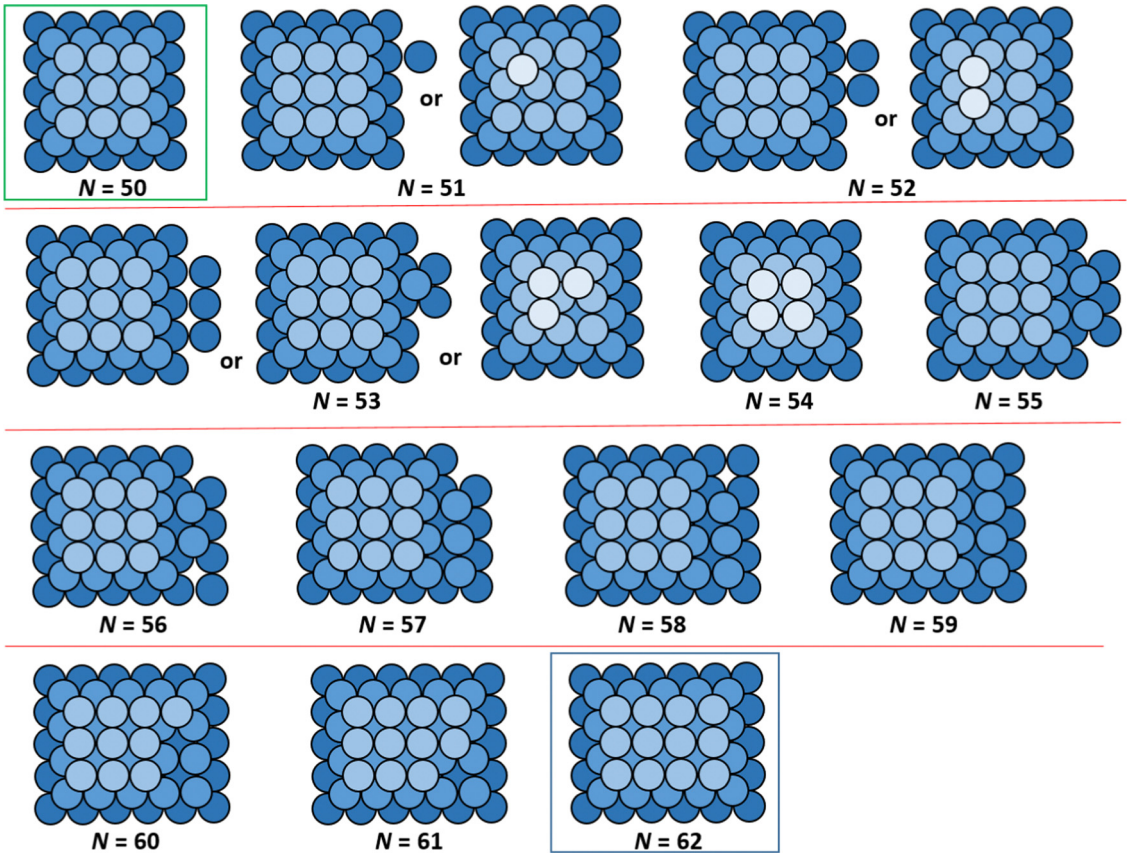

Fig. 2 Examples of ground state configurations (top down view) of supported NCs between closed-shell TP sizes N = 50 and N = 62. Degenerate ground state configurations are also shown.

possible NC heights, k, as well as by listing the different possible numbers of atoms, N_{base}, in the base layer of the ground state NCs configurations. We also list the total energy for the ground state of the supported NCs, E_N (relative to that for gaseous metal atoms and a metal-free support surface), in units of ϕ. Note that total interaction of each base layer atom with the support surface is $-4f\phi = -3\phi$, so conveniently values of E_N/ϕ are all negative integers. Table 1 also lists the quantity $\Delta E_N = E_N - E_{N-1}$, where $\Delta E_N = -6\phi$, -5ϕ, or -4ϕ takes just three values. ΔE_N is a key component in the determination of the adatom formation energy, $E_{\text{form}}(N)$ (which is also listed in Table 1), and thus in determination of the density, n_{eq}, of mobile surface adatoms in our refined-MF treatment.

NC diffusivity also depends on the specification of hopping dynamics of surface adatoms. Our stochastic model allows hops of under-coordinated surface adatoms to unoccupied NN fcc crystalline sites, which are still connected to the NC. Hop rates, $h = \nu \exp[-\beta E_{\text{act}}]$, have an Arrhenius form where $\nu \approx 10^{12.5}$ s^{-1} is a prefactor or attempt frequency chosen to be identical for all hops. Most modeling of 3D crystalline NC evolution has used a standard bond-breaking or so-called Initial Value Approximation (IVA) prescription of the local environment-dependent activation barrier, E_{act}.[11] However, this and other generic prescriptions fail qualitatively to capture realistic barriers for fcc metals.[11,21] In contrast, we used a refined Brønsted–Evans–Polanyi (BEP) formalism which allows sufficient flexibility in the specification of E_{act} to recover DFT values for various key diffusion processes. See ref. 12, 27 and 28 for details. In the model with parameters for Ag, we recover $E_d(100) = 0.425$ eV and $E_d(111) = 0.10$ eV for terrace diffusion on {100} and {111} facets, respectively, and $E_e(100) = 0.275$ eV and $E_e(111) = 0.30$ eV for edge diffusion along {100} and {111} micro-faceted steps, respectively.

It is appropriate to comment further on our prescription of mass transport. Hopping of under-coordinated surface atoms to neighboring crystalline sites has been the default prescription for effective modeling of homoepitaxial film growth and relaxation,[24,25] as well as for surface-diffusion mediated evolution of unsupported metal NCs.[29–31] Diffusion across monolayer steps and facets boundaries (particularly from one {111} side facet to an adjacent one) can impact diffusion of supported NCs. Such process occur *via* a sequence of hops to NN fcc crystalline sites. See the ESI.† An additional Ehrlich–Schwoebel (ES) barrier for interlayer transport above that for terrace diffusion across {111} facets of 0.1 eV is also incorporated (for Ag NCs). As an aside, interlayer diffusion sometimes involves atom exchange rather than hopping. However, for the modeling to accurately capture NC structure evolution, it is only necessary to correctly incorporate the rate of this process rather than the mechanism, and our selection of ES barriers is made to achieve this goal. For diffusion around the NC base, we relax the constraint that atoms hopping to available NN fcc

Table 1 Illustrative results for the lattice-gas model with $f = 0.75$ for {100} epitaxially-supported 3D fcc metal clusters sizes $N = 50–65$: ground state configurations and energetics, E_N and $\Delta E_N = E_N - E_{N-1}$, as well as formation energies, $E_{form}(\alpha)$ for adatoms on the top ($\alpha = 100$) and side ($\alpha = 111$) facets, and at the perimeter of the NC base (α = base). (See Section 3.1 for details where it is shown that $E_{form}(100) = E_{form}$(base) for $f = 0.75$) NC sizes, N, corresponding to closed-shell TP, where D_N has deep local minima, as well as where D_N has local maxima are indicated in bold italic font. A comprehensive analysis for NC sizes $N = 13–126$ is provided in the ESI

N	N_{base}	k	$-E_N/\phi$	$-\Delta E_N/\phi$	$E_{form}(100)/\phi = E_{form}$(base)$/\phi$	$E_{form}(111)/\phi$	D_{700K}
50	***5 × 5 = 25***	***3***	***251***	***6***	***2***	***3***	***min***
51	25, 26	3, 4	255	4	0	1	
52	25, 27	3, 4	260	5	1	2	
53	***25, 27, 28***	***3, 4***	***265***	***5***	***1***	***2***	***max***
54	5 × 5 = 25	4	271	6	2	3	
55	28	3	276	5	1	2	
56	29	3	281	5	1	2	
57	29	3	287	6	2	3	
58	30	3	292	5	1	2	
59	30	3	298	6	2	3	
60	30	3	303	5	1	2	
61	30	3	309	6	2	3	***~min***
62	***5 × 6 = 30***	***3***	***315***	***6***	***2***	***3***	***min***
63	30, 31	3, 4	319	4	0	1	
64	30, 32	3, 4	324	5	1	2	
65	***30, 32, 33***	***3, 4***	***329***	***5***	***1***	***2***	***max***

sites must remain connected to the NC. Specifically, atoms can hop to second NN sites at the corner of the rectangular base of an NC, thereby allowing rounding of the corner from one side to another of the faceted NC. See the ESI.† (This atom rounding the corner still has 4 NN substrate atoms, thus avoiding a high energy configuration associated with an atom hopping to a site with no NN higher in the NC.) For corner rounding at the base, there is an additional ES barrier relative to edge diffusion along the base of 0.1 eV.

KMC simulation of Ag NC diffusion is then performed where surface hopping processes are implemented with probabilities proportional to the physical rates using a rejection-free algorithm. The diffusion coefficient, D_N, is obtained by tracking the lateral mean-square displacement of the center of mass of the NC as a function of time. Fig. 3 presents illustrative results from previously performed KMC simulations[22] for D_N *versus* N for Ag NCs at 700 K. We note that similar behavior has been observed in simulations for diffusion of supported Pt NCs.[32] The strong oscillatory decay with local minima at or near certain closed-shell TP sizes will motivate subsequent discussion and analysis. In this contribution, we will compare results from our refined MF theory (also shown in Fig. 3), and from a beyond-MF treatment, with those from KMC analysis.

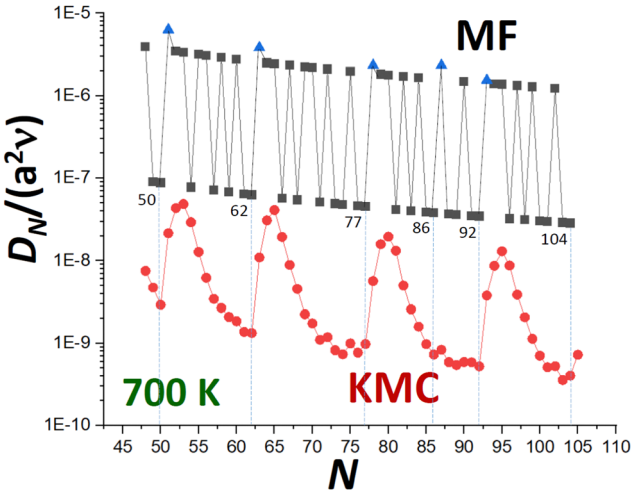

Fig. 3 KMC simulation results (circles) for D_N *versus* N for {100} epitaxially-supported Ag NCs at 700 K for $N = 48–105$. Also shown are predictions from a somewhat simplified version of a refined MF treatment (squares). Blue triangles indicate MF values for sizes $N = N_{cs} + 1$ where there are particular issues with MF. Vertical dashed lines correspond to close-shell NC sizes, N_{cs}.

Refined-MF treatment for diffusion of faceted NCs

Overview

The MF formulation described above requires adaption to provide a reasonable treatment of the diffusion of the faceted epitaxial NCs in our model. It is important to recognize that the density of mobile adatoms per adsorption site on the {100} top facet, n_{100}, the {111} side facets, n_{111}, and also at sites along the base contact line, n_{base}, differ primarily due to different adatom formation energies. Below we use α or $\alpha' = 100$, 111, or "base" to label these three cases. The adatom densities will be denoted by n_α and the formation energies by $E_{form}(\alpha)$, where $n_\alpha \propto \exp[-\beta E_{form}(\alpha)]$, and where both quantities depend on α and on NC size. The formation energy, $E_{form}(\alpha)$ corresponds to the minimum energy cost to extract an atom from a highly-coordinated site (generally a kink site) in a ground state configuration of the NC, and move it onto the desired facet or to the perimeter of the NC base. Note that the coordination of this atom to be extracted is given by the quantity $|\Delta E_N|/\phi$ listed in Table 1, and this coordination depends on NC size, N. Since $|\Delta E_N|$ also corresponds to the energy cost to entirely remove an atom to the vapor phase from such a site in a NC of size N, it follows that

$$E_{form}(\alpha) = |\Delta E_N| - |E_{ads}(\alpha)|, \text{ with } E_{ads}(\alpha) = -m_\alpha \phi, \text{ for NC size } N, \quad (2)$$

where $E_{ads}(\alpha)$ is the adsorption energy for case α. One has that $m_{100} = 4$ ($m_{111} = 3$) for adsorption at 4-fold (3-fold) hollow sites on {100} ({111}) facets; also $m_{base} = 4f + 1$ as an adatom at the base perimeter has 4 bonds of strength $f\phi$ to the substrate, and one lateral bond of strength ϕ to another atom in the NC. Thus, for our model with $f = 0.75$, adatoms on {100} facets and at the base perimeter just happen to have the same E_{form}. Again, these different formation energies (and also different configurational entropy factors discussed below) result in the above-mentioned different densities.

Diffusion barriers, $E_d(\alpha)$, for mobile surface adatoms also depend on α. For Ag NCs, one has that $E_d(100) = 0.425$ eV and

$E_d(111) = 0.10$ eV on {100} and {111} facets, respectively; $E_d(\text{base}) = E_e(100) = 0.275$ eV for edge diffusion along {100} micro-faceted steps at the NC base. Thus, the corresponding hop rates $h_\alpha = \nu \exp[-\beta E_d(\alpha)]$ for these mobile surface adatoms also depend on α.

In our refined MF treatment, we will separately account for the contribution of these three different classes of mobile surface adatoms to NC diffusion. Below, we let A_{100}, A_{111}, and A_{base} denote the number of adsorption sites on the top {100} facet, on all four side {111} facets, and around the base, respectively. For adatoms on the top {100} facet and at the base, one has a lateral change in the NC center of mass of $\delta R_{CM} = a/N$ for each hop. Thus, the corresponding contributions to D_N are

$$D_N(100) = a^2 h_{100} n_{100} A_{100}/N^2 \text{ and } D_N(\text{base}) = a^2 h_{\text{base}} n_{\text{base}} A_{\text{base}}/N^2. \quad (3)$$

For adatoms on the {111} side facets, the two lateral hops of the 6 possible hops between fcc(111) adsorption sites have a lateral $\delta R_{CM} = a/N$, but the other 4 have a lateral $\delta R_{CM} = 2^{-1/2} a/N$. Then, appropriate random walk analysis (see the ESI†) shows that the contribution to D_N is

$$D_N(111) = (2/3) a^2 h_{111} n_{111} A_{111}/N^2. \quad (4)$$

Combining these three contributions gives the total D_N. We comment below on possible further modification to incorporate the effect of ES barriers.

From (3) and (4), it is clear that for each α, we can associate an effective barrier, $E_{\text{eff}}(\alpha) = E_d(\alpha) + E_{\text{form}}(\alpha)$, for transport across the relevant facet or around the base. Values for these effective barriers are reported in Table 2 for Ag NCs revealing that $E_{\text{eff}}(111)$ and $E_{\text{eff}}(\text{base})$ are significantly lower that $E_{\text{eff}}(100)$. This indicates that that contributions to D_N from transport across {111} side facets and around the base of the NC dominate those from transport across the {100} top facet.

To more clearly show the NC size scaling of D_N, it is convenient to consider a subset of perfect closed-shell TPs of k layers with a top $k \times k$ atom {100} facet, and thus a $(2k-1) \times (2k \times 1)$ bottom {100} layer, *i.e.* $\text{TP}_{(2k-1)\times(2k-1),k}$. For these TP, which most closely mimic the continuum Winterbottom shape, one has that

$$N = k(2k-1)(7k-1)/6,\ A_{100} = (k-1)^2,\ A_{111} = 2k(3k-1), \text{ and } A_{\text{base}} = 4(2k-1). \quad (5)$$

Thus, in the large k or large N regime, one has that

$$A_{100} \sim (3N/7)^{2/3},\ A_{111} \sim 6A_{100}, \text{ and } A_{\text{base}} \sim 8(3N/7)^{1/3}. \quad (6)$$

As a result, combining the above contributions to D_N, one concludes that

$$D_N \approx (3/7)^{2/3} a^2 N^{-4/3} [h_{100} n_{100} + 4 h_{111} n_{111} + 8(3N/7)^{-1/3} h_{\text{base}} n_{\text{base}}]. \quad (7)$$

Finally, we identify one self-evident limitation regarding the utility of the MF formulation. Consider NCs whose size exceeds that for structures with closed-shell ground states by one, *i.e.*, $N = N_{cs} + 1$. Then, the ground state structure already has one isolated adatom either on the {100} top facet or at the base. The formation energies, $E_{\text{form}}(100) = E_{\text{form}}(\text{base}) = 0$ vanish, and the adatom densities $n_{100} \approx n_{\text{base}} \approx 1/(A_{100} + A_{\text{base}})$ on {100} facets and at the base are correspondingly "anomalously" high. However, these high densities do not correlate with correspondingly high NC diffusivity. In these cases, NC dynamics primarily involves this isolated atom moving around a static closed-shell "core" of the NC, which in itself does not result in NC diffusion.

Analysis of adatom densities n_α including entropic effects

A detailed analysis of the mobile adatom densities, $n_\alpha = n_{100}$, n_{111}, or n_{base}, is possible utilizing a standard statistical mechanical formalism to determine the probability that the system is in an energetically excited state with such an adatom at the desired location. The analysis below does not apply for the cases $N = N_{cs} + 1$ (where as noted above, there is already a surface adatom in the ground state), or for $N = N_{cs} + 2$ where slight refinement of the following analysis is needed. See the ESI.† Let Ω_N denote the degeneracy of the ground state of the NC with N atoms and energy E_N. Then, the degeneracy of the "excited state" configuration where an atom is shifted from this ground state to a lower-coordinated adsorption site of type α is $\Omega_{N-1}\, A_\alpha$, and the energy of this excited state is $E_{N-1} + E_{\text{ads}}(\alpha)$. Thus, the canonical partition function for the NC of N atoms becomes

$$Q_N = \Omega_N \exp[-\beta E_N] + \Omega_{N-1} \textstyle\sum_{\alpha'} A_{\alpha'} \exp[-\beta\{E_{N-1} + E_{\text{ads}}(\alpha')\}] + \ldots \quad (8)$$

The implicit terms reflect the more highly excited states of the NC. Then, the probability, P_α, that the NC is in an excited state with exactly one mobile adatom on an adsorption site of type α is given by

$$P_\alpha = \Omega_{N-1} A_\alpha \exp[-\beta\{E_{N-1} + E_{\text{ads}}(\alpha)\}]/Q_N. \quad (9)$$

We consider the regime of temperatures and relatively small NC sizes where the system is most likely in the ground state (so the first term in Q_N dominates), and where it is unlikely that there is more than one mobile adatom on a side or top facet or at the base. Then, it follows that the density of such atoms on adsorption site type α satisfies

$$n_\alpha \approx P_\alpha/A_\alpha \approx (\Omega_{N-1}/\Omega_N)\exp[\beta\{E_N - E_{N-1} - E_{\text{ads}}(\alpha)\}] = (\Omega_{N-1}/\Omega_N)\exp[-\beta E_{\text{form}}(\alpha)]. \quad (10)$$

Table 2 Effective barriers, $E_{\text{eff}}(\alpha)$, for different mass transport pathways (*i.e.*, diffusing adatoms on different facets, *etc.*), α, for Ag NCs

$E_{\text{eff}}(\alpha)$ in eV	α = top {100}	α = side {111}	α = base
$N = N_{cs}$ & some other N	0.875	0.775	0.725
[a] $N = N_{cs} + 1$ (mostly)	0.425	0.325	0.275
$N = N_{cs} + 2,3$ (mostly)	0.650	0.550	0.500

[a] As noted in the text, the barriers listed for $N = N_{cs} + 1$ do not correlate with NC diffusion.

Again, there are special cases where this formalism must be modified. Thus, to determine n_α, in addition to $E_{form}(\alpha)$, which is reported in Table 1, it is appropriate to determine configurational degeneracies. However, the factor Ω_{N-1}/Ω_N is typically of order unity, so that the approximation $n_\alpha \approx \exp[-\beta E_{form}(\alpha)]$ is generally reasonable.

Refined-MF predictions for D_N *versus* KMC results

Refined-MF analysis for $N = N_{cs}$ (low D_N) and $N = N_{cs} + j$ with j = 1–3 (high D_N)

Motivated by the results for NC diffusivity shown in Fig. 3, we initially focus on special NC sizes, $N = N_{cs}$ (for closed-shell TP ground states) where D_N generally exhibits local minima, and sizes $N = N_{cs} + j$ with j = 1, 2, or 3, noting that KMC values for D_N exhibit local maxima for $N = N_{cs} + 3$ (and values for $N = N_{cs} + 2$ are only slightly lower). These cases are analyzed in detail separately below. We present refined-MF results for D_N for N_{cs} = 50, 62, 77, and 92, and directly compare these with accurate results from KMC simulation.

(i) For $N = N_{cs}$, the NCs have non-degenerate ground states, so that $\Omega_N = 1$. One also has that $\Omega_{N-1} = 4$ corresponding to removing an atom from one of the 4 corners of the top {100} facet on the perfect TP. Since $E_{form}(100) = E_{form}(\text{base}) = 2\phi$ and $E_{form}(111) = 3\phi$ (see Table 1), one has from (10) that

$$n_{100} = n_{base} = 4\exp[-2\beta\phi] \text{ and } n_{111} = 4\exp[-3\beta\phi]. \quad (11)$$

Since the $E_{form}(\alpha)$ are largest for these cases, it follows that n_α adopt the lowest possible values. Thus, the refined-MF formulation predicts particularly low diffusivity for these cases, consistent with KMC results.

(ii) For $N = N_{cs} + 1$, we have already noted above that this is an anomalous case as the ground state structure already has one isolated adatom adsorbed on the {100} top facet or at the base of a closed-shell "core". Thus, one has that E_{form}(100 or base) = 0, and $n_{100} = n_{base} = 1/(A_{100} + A_{base})$ are correspondingly high. Additional analysis reveals that $n_{111} = n_{base}\exp[-\beta\phi]$. See the ESI.† This allows determination of the refined-MF predictions for diffusivity which are artificially high, corresponding to local maxima with respect to N, in contrast to KMC results.

(iii) For $N = N_{cs} + 2$, the ground state consists of a dimer adsorbed on the {100} top facet (for $N_{cs} \geq 18$), or at the base of a closed-shell "core". A feature specific to this case is that when the dimer dissociates, it creates two mobile adatoms. As a result, some refinement of the formulation leading to the prefactor in (10) is required. See the ESI.† Since typically $E_{form}(100) = E_{form}(\text{base}) = \phi$ and $E_{form}(111) = 2\phi$ from Table 1, ignoring the prefactors it follows that

$$n_{100} = n_{base} \sim \exp[-\beta\phi] \text{ and } n_{111} \sim \exp[-2\beta\phi], \quad (12)$$

which are substantially higher than for $N = N_{cs}$.

(iv) For $N = N_{cs} + 3$, the ground state usually consists of a trimer adsorbed on the {100} top facet (for $N_{cs} \geq 18$) or at the base of a closed-shell "core". Then, Ω_N corresponds to the number of locations on the core of a linear or bent trimer on the top {100} facet plus the number of locations of a linear or triangular trimer at the base. Ω_{N-1} corresponds to the number of locations on the core of a dimer. See the ESI,† for more details. These degeneracies can be readily determined in specific cases. Since typically $E_{form}(100) = E_{form}(\text{base}) = \phi$ and $E_{form}(111) = 2\phi$ from Table 1, it then follows that

$$n_{100} = n_{base} \approx (\Omega_{N-1}/\Omega_N)\exp[-\beta\phi] \text{ and } n_{111} \approx (\Omega_{N-1}/\Omega_N)\exp[-2\beta\phi], \quad (13)$$

again substantially higher than for $N = N_{cs}$.

It is clear that the refined-MF treatment will capture aspects of the oscillatory trend in D_N *versus* N shown in KMC simulation with local minimum values at $N = N_{cs}$ substantially below similar high values at $N = N_{cs} + 2$ and $N = N_{cs} + 3$. As noted above, refined-MF values for $N = N_{cs} + 1$ are artificially high corresponding to local maxima (in contrast to KMC). Table 3 compares refined-MF D_N values at 700 K from (3) and (4) incorporating detailed evaluation of A_α and n_α with accurate KMC values. This is done for various closed-shell NC sizes, N_{cs} = 50, 62, 77, and 92. As already indicated above, contributions to D_N from transport across {111} side facets and around the base of the NC dominate those from transport across the {100} top facet. This dominance primarily reflects the lower effective barriers, $E_{eff}(\alpha)$ for α = 111 and α = base *versus* α = 100 (see Table 2), but also partly reflects entropic factors.

It is clear that the refined-MF treatment is reasonably effective in predicting the relative values of D_N at local minima at $N = N_{cs}$ and the much higher values for $N = N_{cs} + 2$ and $N = N_{cs} + 3$ (the latter being a local maximum for KMC). The refined-MF treatment does not capture the more subtle feature that accurate KMC values for $N = N_{cs} + 2$ are slightly lower (not higher) than those for $N = N_{cs} + 3$. It should be emphasized, however, that all refined-MF values are roughly two orders of magnitude above those from KMC. As noted above, this discrepancy could be partly ameliorated by incorporating an additional universal factor, $\exp[-\beta\delta]$ in the refined-MF D_N which reflects an additional ES type barrier, $\delta > 0$, for transport between different sides of the NC. However, we argue that the discrepancy primarily reflects the fundamental shortcoming that the refined-MF treatment greatly under-estimates the effective barrier for NC diffusion, as will be discussed in detail within the framework of beyond-MF treatments.

Table 3 Comparison of refined-MF and KMC predictions for diffusivity, $D_N/(a^2\nu)$, for selected NC sizes $N = N_{cs}$ (corresponding to local minima) and for $N = N_{cs} + j$ with j = 1–3 (which include local maxima). See Fig. 3. Entries in the table should be multiplied by 10^{-9} for KMC, and 10^{-7} for the refined MF treatment

	Refined-MF $D_N/(a^2\nu)$ ($\times 10^{-7}$)				KMC $D_N/(a^2\nu)$ ($\times 10^{-9}$)			
	N_{cs}	$N_{cs}+1$	$N_{cs}+2$	$N_{cs}+3$	N_{cs}	$N_{cs}+1$	$N_{cs}+2$	$N_{cs}+3$
N_{cs} = 50	3.31	57.54	37.29	23.07	2.91	21.61	43.53	48.75
N_{cs} = 62	2.40	36.01	24.92	17.12	1.33	10.95	30.92	41.12
N_{cs} = 77	2.03	22.01	17.21	12.50	0.98	5.66	15.84	19.60
N_{cs} = 92	1.59	14.67	12.60	9.71	0.53	3.79	8.63	13.01

Approximate refined-MF analysis for all NC sizes *versus* KMC results

Here, we explore an approximate version of the refined-MF treatment which has the advantage of providing a convenient general formula for D_N. To this end, we utilize a simplified form (7) which already incorporates approximations for A_α, but now we also include additional reasonable approximations for adatom densities which neglect some entropic factors as described below. We thereby obtain

$$D_N/(a^2\nu) \approx (3/7)^{2/3}N^{-4/3}\{\exp[-\beta E_d(100)] + 4\exp[-\beta(E_d(111)+\phi)] + 8(3N/7)^{-1/3}\exp[-\beta E_d(\text{base})]\}n_{\text{base}}, \quad (14)$$

using $n_{\text{base}} = n_{100}$ and $n_{111} = \exp[-\beta\phi]n_{\text{base}}$. For all $N \neq N_{cs} + 1$, we use $n_{\text{base}} \approx \exp[-\beta E_{\text{form}}(\text{base})]$ where the N-dependent $E_{\text{form}}(\text{base}) = E_{\text{form}}(100) = |\Delta E_N| - 4\phi$ is listed in Table 1 for a narrow range of N, and in the expanded Table in the ESI,† for a broader range of N = 13–126. For $N = N_{cs} + 1$, we use $n_{\text{base}} = 1/(A_{100} + A_{\text{base}})$. The first term with $E_d(100) = 0.425$ eV is clearly dominated by the second term with $E_d(111) + \phi = 0.325$ eV, and also by the third term with $E_d(\text{base}) = 0.275$ eV.

In Fig. 3, we have compared the predictions of (14) with accurate KMC values for D_N. As expected, the simplified MF form (14) effectively captures the local minima of D_N for $N = N_{cs}$, and much higher values for $N = N_{cs} + 2$ and $N = N_{cs} + 3$. However, (14) produces "excessive" oscillatory behavior of D_N reflecting the rapid oscillatory variation in $E_{\text{form}}(N)$, although (14) does captures the slow overall decrease in the oscillatory D_N with increasing N. Again, MF values of D_N are substantially above KMC values, a shortcoming elucidated by a beyond-MF analysis.

Beyond-MF analysis for D_N *versus* MF and KMC results

Overview

The above results reveal that refined-MF theory fails to reliably describe detailed trends in NC diffusivity with size, and also thus fails to elucidate the relationship between NC structure and diffusivity. However, this structure-diffusivity relationship can be elucidated and captured by a beyond-MF analysis tailored to the diffusion of epitaxially-supported faceted NCs. In this section, we outline such a beyond-MF analysis which recognizes that the diffusion of such NCs is controlled by a cooperative multi-step mechanism wherein the outer layer of a facet on one side of the NC is disassembled and those adatoms transferred to form (*i.e.*, to nucleate and grow to completion) a new outer layer on a target facet another side of the NC.[19] See Fig. 4. This picture of a cooperative multi-step mechanism contrasts the MF assumption that NC diffusion results from (non-cooperative) independent random hopping of surface atoms. It should also be noted that such cooperative nucleation and growth type processes have also been identified as underlying the shape equilibration of faceted fcc metal NCs with initial non-equilibrium shapes.[12,27–31,33]

Our beyond-MF analysis will naturally consider the change in system energy, $\delta E(q)$, as a function of the number, q, of atoms transferred from the facet which is being disassembled to the target facet on another side of the NC. $\delta E(q)$ will generally quickly increase from zero as q increases above zero and will then return to zero once a new outer layer of the target facet is completed on another side of the NC, or when the NC returns to a configuration identical to the initial configuration but shifted by a surface lattice constant.

Some aspects of the definition and determination of $\delta E(q)$ should be mentioned. First, values of $\delta E(q)$ for integer q will correspond to the change in energy after completion of transfer of the qth atom, *i.e.*, after its incorporation at an adsorption site at the base of the target facet if $q = 1$, or after its incorporation into a 2D cluster of atoms forming on the target facet for $q > 1$. We will also define $\delta E(q)$ for half-integer values of q. The value for say $q = n + 0.5$ for integer n, corresponds to the change in system energy when the $(n + 1)$st atom has been detached from the facet being disassembled, but is not yet incorporated into a 2D cluster of $n + 1$ atoms on the target facet. The strength of the adsorption energy of this isolated mobile atom which is in transit is taken to be 3ϕ corresponding to adsorption on a {111} facet, or at a corner site at the base of the NC. Second, for the

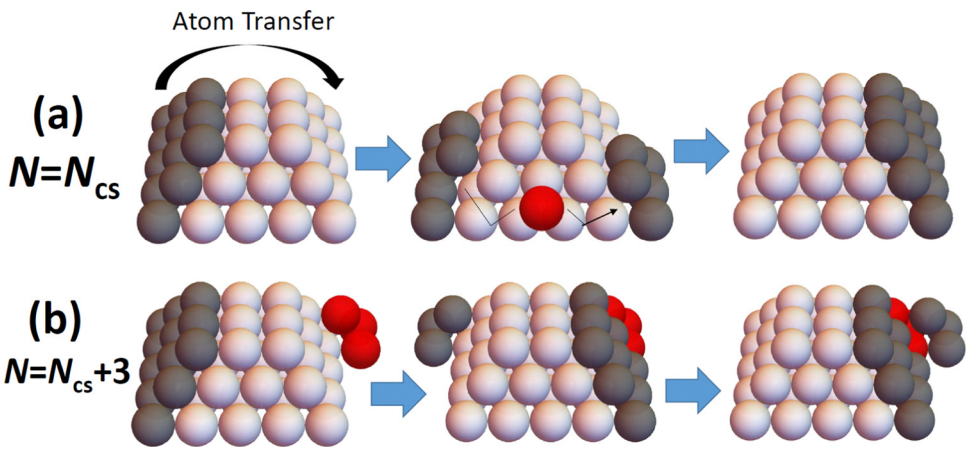

Fig. 4 Schematic of disassembly and reformation of outer layers of facets on: (a) perfect; and (b) imperfect TPs. N_{cs} = 50 for the cases shown.

above mass transfer process, one considers the specific scenario where atoms are removed from the disassembling outer layer of one side facet in a way which minimizes the number of broken bonds, and added to the growing 2D cluster forming the new outer layer on another side facet in order to maximize the number of bonds formed. Such a process will minimize $\delta E(q)$ for each q, and thereby generate the minimum energy path (MEP) for facet disassembly and formation. Third, it should be emphasized that $\delta E(q)$ is associated with energetic changes at $T = 0$ K rather than free energy changes, $\delta F(q)$, for $T > 0$. The latter would also account for the influence of changes in configurational entropy to more accurately capture the effective barrier.

The effective barrier, $E_{\text{eff}} = E_{\text{eff}}(N)$ for disassembling and forming outer layers of facets, and thus for NC diffusion, will be controlled by $\delta E_{\max} = \delta E_{\max}(N) = \max_q \delta E(q)$ for this MEP. If one neglects entropic effects, one can then identify $E_{\text{eff}}(N) = E_{\text{diff}} + \delta E_{\max}(N)$, where E_{diff} is an appropriate diffusion barrier for mobile surface atoms. Adatom diffusion across the top {100} facet should not contribute significantly to NC diffusion given the high terrace diffusion barrier $E_d(100) = 0.425$ eV. Thus, we choose a lower value of $E_{\text{diff}} \approx 0.15$ eV reflecting a combination of transport across {111} facets and around the NC base with possible ES effects. In summary, the effective barrier, $E_{\text{eff}}(N)$, for NC diffusion is actually controlled by the entire MEP for the cooperative multi-step process of disassembly and formation of outer layers on the faceted NC. This contrasts the barrier(s) in the MF treatment which are associated with the "single-step" process of forming a mobile surface adatom on various facets or at the NC base.

Detailed analysis of $\delta E(q)$ *vs.* q and of $\delta E_{\max}(N)$ for $N = N_{\text{cs}} + j$ with $j = 0$–3

Next, we provide a detailed analysis of $\delta E(q)$ *versus* q, extracting the associated $\delta E_{\max}$, and focusing on comparison of cases $N = N_{\text{cs}}$ (closed-shell sizes often with local minima in D_N) and $N = N_{\text{cs}} + j$ for $j = 1$–3 (with higher D_N). For specificity, in Fig. 5, we show $\delta E(q)$ *versus* q for $N = N_{\text{cs}} + j$ with $j = 0$, 1, 3, where $N_{\text{cs}} = 50$. This closed-shell NC size corresponds to a truncated pyramid $TP_{5\times5,3}$.

For $N = N_{\text{cs}} = 50$, the outer layer of a complete side facet is composed of $q_{\max} = 12$ atoms, and consequently Fig. 5 shows the MEP $\delta E(q)$ for $0 \le q \le q_{\max} = 12$. This $\delta E(q)$ initially increases quickly (as mentioned above), and is symmetric about $q = q_{\max}/2$, and shows that $\delta E_{\max}(N = 50) = 6\phi$. Details of NC configurations *versus* the number q of atoms transferred are shown in the ESI.†

For $N = N_{\text{cs}} + j$ with $j > 0$, a cluster of j atoms already exists on one facet, which reduces the energy cost $\delta E(q)$ relative to $j = 0$ for transferring atoms from another perfect facet to grow a 2D cluster and complete a new layer on that target facet. Furthermore, to complete that layer, one now needs to transfer only $q_{\max} - j$ atoms. These features are shown in Fig. 5 which also presents $\delta E(q)$ *versus* q for $j = 1$ ($N = 51$) where $\delta E_{\max}(N = 51) = 5\phi$, and for $j = 3$ ($N = 53$) where $\delta E_{\max}(N = 53) = 4\phi$. The case $j = 2$ ($N = 52$) is not shown to avoid overcrowding the plot, but in this

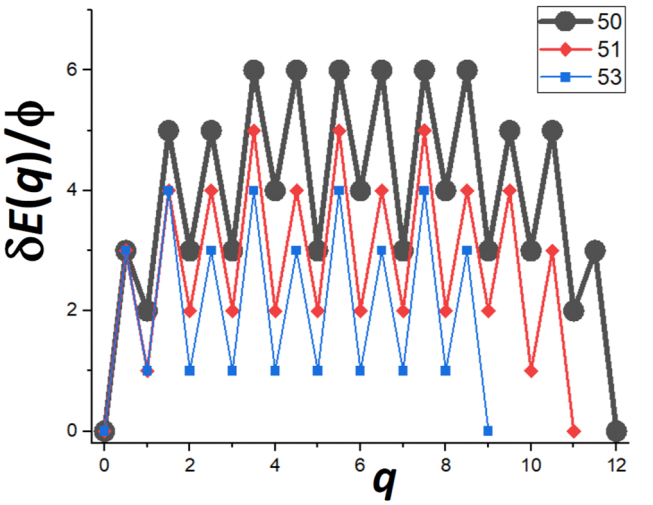

Fig. 5 $\delta E(q)$ *versus* q for $N = 50$, 51, 53 (*i.e.*, for $N = N_{\text{cs}} + j$ with $j = 0$, 1, and 3 with $N_{\text{cs}} = 50$ corresponding to $TP_{5\times5,3}$). $\delta E_{\max} = 6\phi$, 5ϕ, and 4ϕ for $N = 50$, 51, and 53 (& 52), respectively.

case one has that $\delta E_{\max}(N = 52) = 4\phi$ as for $N = 53$. As a final remark for cases with $j > 0$, a small cluster of j atoms is left behind on the disassembled facet (see Fig. 4b). However, there is a relatively low cost to transfer this cluster to another side facet recovering a shifted version of the initial NC configuration. This portion of the MEP is not shown in Fig. 5. Consequently, this feature does not impact the effective barrier, $E_{\text{eff}}(N) = E_{\text{diff}} + \delta E_{\max}(N)$, for NC diffusion.

To summarize the above analysis, a local maximum occurs in $\delta E_{\max}$ for $N = N_{\text{cs}}$, with $\delta E_{\max}$ lower for $N = N_{\text{cs}} + 1$, and lowest for $N = N_{\text{cs}} + 2$ or $N = N_{\text{cs}} + 3$. This corresponds to local minima of D_N at $N = N_{\text{cs}}$ and local maxima at $N = N_{\text{cs}} + 3$ (with just slightly lower values for $N = N_{\text{cs}} + 2$). While these trends are only illustrated above for $N_{\text{cs}} = 50$, they actually apply for general N_{cs}. This analysis effectively elucidates a NC structure – diffusivity relationship. Perhaps not surprisingly, NCs with $N = N_{\text{cs}}$ and ground-state closed-shell TP structures have low diffusivity, reflecting the higher energy cost to disassemble and reassemble outer layers of side facets. Next, consider NCs where the ground state structure includes a closed shell TP core, but also additional atoms which form a 2D cluster on a side facet. Here, the presence of the additional 2D cluster lowers the energy cost of disassembling and reassembling outer layers of side facets, and thus enhances diffusivity relative to the case with $N = N_{\text{cs}}$.

As an aside, we note that in general, NC structure-diffusivity relationships can be subtle. Note from Fig. 3 that NCs for sizes just below closed-shell sizes generally have D_N comparable to "local minima" for $N = N_{\text{cs}}$ (and actually sometimes even slightly lower D_N as is the case, *e.g.*, for $N_{\text{cs}} = 77$). Below, we show examples where for such sizes, $\delta E_{\max}$ has the same local maximum value as for the closed-shell size, which does straightforwardly explain the low value of D_N. Another observation regarding subtle NC structure – diffusivity relationships is that for single-atomic-layer 2D epitaxially-supported NCs, closed-shell structures do not correspond to local minima in

diffusivity.[34,35] This feature reflects the stronger influence of entropic over energetic factors in these 2D systems in determining D_N *versus* N.

Note that the MEP for $TP_{5\times5,3}$ with $N_{cs} = 50$, and $TP_{5\times6,3}$ with $N_{cs} = 62$, should be identical. For $TP_{5\times6,3}$, the outer layer on a {111} side facet with base length 5 and height 3 (just as for $TP_{5\times5,3}$) can disassemble, forming a new outer layer on an adjacent {111} side facet with initial base length 6 which upon completion of this process will have a base length 5. Repeating this process for $TP_{5\times6,3}$ induces NC diffusion. Likewise, MEPs are identical for $TP_{6\times6,3}$ with $N_{cs} = 77$, and $TP_{6\times7,3}$ with $N_{cs} = 92$, *etc.*

Trend in $\delta E_{max}(N)$ for increasing N

Next, we show that apart from oscillations in D_N and $\delta E_{max}(N)$ as N varies between consecutive closed-shell sizes, there is an overall increase without bound in $\delta E_{max}(N)$ as N increases (in marked contrast to MF behavior). Specifically, we focus on a special subset of "ideal" closed-shell sizes mentioned previously. These correspond to truncated pyramids, $TP_{(2k-1)\times(2k-1),k}$, where the length of the edge of the top {100} facet and the edge between adjacent {111} side facets are equal (to k atoms). As a result, these structures best mimic the continuum Winterbottom shape shown on Fig. 1 for $f = 0.75$. Fig. 6 shows the behavior of the "upper envelope" of $\delta E(q)$ *versus* q for cases with $k = 2, 3, 4, 5, 6, 7, \ldots$ where $N = 13, 50, 126, 255, 451, 728, \ldots$ and the number of atoms in the outer layer of a single {111} side facet of $q_{max} = 5, 12, 22, 35, 51, 70, \ldots$, respectively. The "upper envelope" just corresponds to values of $\delta E(q)$ for half-integer q associated with states where an atom is in transition between the side facet being disassembled and the target facet on which a new layer is being formed. These $\delta E(q)$ exceed those for adjacent integer values of q (*cf.* Fig. 5), and thus suffice to determine δE_{max}. From Fig. 6, we find that $\delta E_{max} = 4\phi, 6\phi, 8\phi, 9\phi, 11\phi$, and 13ϕ, for $k = 1$–7, respectively. These results reflect the feature that δE_{max} increases roughly linearly with increasing NC height, k (or with NC width or edge length) for ideal closed-shell TPs. Thus, MEP analysis predicts that the effective barrier, $E_{eff}(N) = E_{diff} + \delta E_{max}(N)$, increases without bound for increasing NC size.

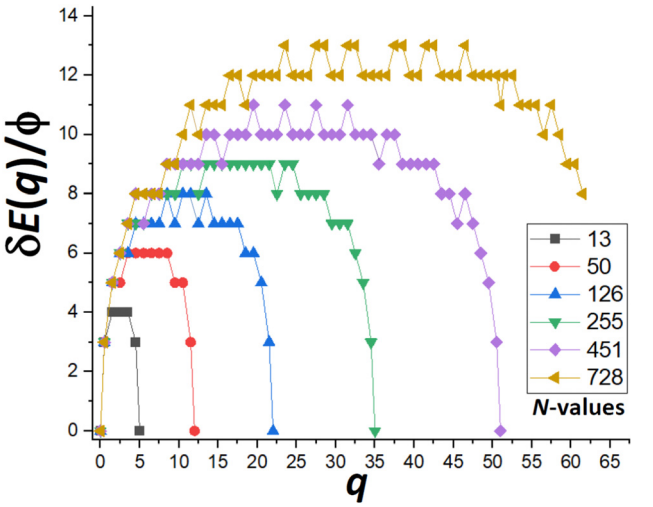

Fig. 6 $\delta E(q)$ *versus* q for $N = 13, 50, \ldots$ indicated in the legend which correspond to $TP_{(2k-1)\times(2k-1),k}$ for $k = 2, 3, \ldots$. $\delta E_{max} = 4\phi, 6\phi, \ldots$ for $N = 13, 50, \ldots$, respectively.

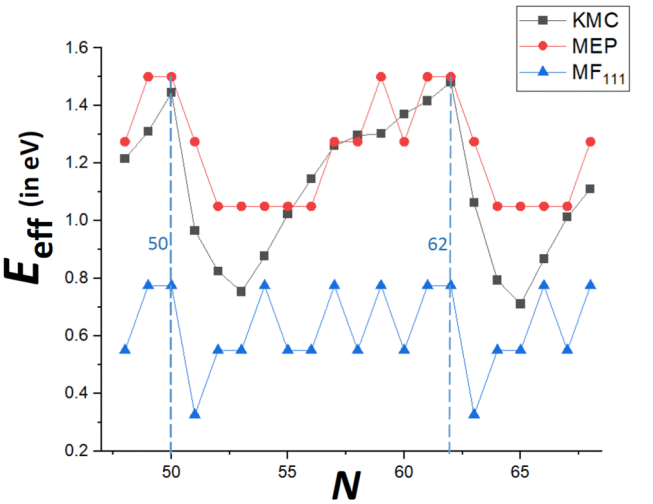

Fig. 7 $E_{eff}(N)$ for Ag NCs with $N = 48$–68 from beyond-MF MEP analysis, KMC simulation, and refined MF analysis. KMC values are determined from behavior of D_N for 700 K $\leq T \leq$ 900 K. Refined-MF predictions correspond to transport on {111} side facets ($\alpha = 111$).

Comparison of beyond-MF MEP with KMC and refined-MF predictions

To demonstrate that our MEP analysis effectively captures the trend in accurate KMC values for $E_{eff}(N)$ *versus* N (particularly for $N = N_{cs} + j$ with $j = 0$–3), both MEP and KMC results are compared in Fig. 7 for $N = 48$–68. Values from the refined-MF treatment are also shown. The MEP analysis reasonably captures the feature that E_{eff} is highest for $N = N_{cs}$, lower for $N = N_{cs} + 1$, but lowest for $N = N_{cs} + 3$ (and gives an equally low value for $N = N_{cs} + 2$). In contrast the refined-MF treatment fails fundamentally as it predicts that E_{eff} for $N = N_{cs} + 1$ is lowest. More generally, MEP results capture the overall oscillatory variation of E_{eff} between closed-shell sizes $N = N_{cs}$. MEP results also include the feature that δE_{max}, and thus E_{eff}, are equal for $N_{cs} = 62$ and $N_{cs} - 1 = 61$, compatible with very similar values of D_N for these sizes. However, KMC values are significantly lower than those from MEP analysis for, say, $N = N_{cs} + j$ with $j = 2$–4. Recall that MEP values come from a $T = 0$ K analysis of energetics rather than a free energy analysis for $T > 0$, and it has been noted that entropic effects can lower the effective barrier for the somewhat similar process of reshaping faceted metal NCs.[33]

Another limitation of the $T = 0$ K MEP analysis of E_{eff} is an inability to distinguish between behavior for $N = N_{cs} + 2$ and $N = N_{cs} + 3$. However, the MEP analysis presented above considered only $\delta E_{max}(N) = \max_q \delta E(q)$. For a more complete analysis to at least elucidate the feature that D_N is higher for $N = N_{cs} + 3$ than for $N = N_{cs} + 2$, one could perform a first-passage time analysis based on the entire MEP profile, $\delta E(q)$ *versus* q. See Fig. 8 for examples of the MEP with $N = 52$ and $N = 53$ corresponding to

$N_{cs} = 50$. In the first-passage time analysis, the system starts in state $q = 0$ at time $t = 0$. Let $P(q, t)$ denote the probability for the NC to be in state q with q transferred atoms at time t, so that $P(q, 0) = 1$ for $q = 0$, and $P(q, 0) = 0$ for $q > 0$. Then, one considers the evolution in time of $P(q, t)$ based upon the set of master equations

$$\mathrm{d}/\mathrm{d}t\, P(q, t) = k^{+}(q - \tfrac{1}{2})P(q - \tfrac{1}{2}, t) + k^{-}(q + \tfrac{1}{2})P(q + \tfrac{1}{2}, t) - [k^{+}(q) + k^{-}(q)]P(q, t). \quad (15)$$

Here $k^{\pm}(q)$ denotes rates to make a transition from state q to state $q \pm \frac{1}{2}$, where these reflect energy barriers along the MEP while satisfying detailed-balance. See the ESI.† In addition, if the total number of atoms transferred is q_{max}, then $q = q_{max} = q_{max}(N)$ is assigned as an absorbing or trapping state (since completing the outer layer of a facet produces a relatively stable configuration) so that $k^{\pm}(q_{max}) = 0$. As a result, $P(q_{max}, t)$ will increase monotonically from 0 to 1, and one can assign a characteristic time $\tau = \tau(N)$ to traverse the MEP and thus to reassemble an outer layer of a side facet *via*, *e.g.*, $P(q_{max}, \tau) = \frac{1}{2}$. Then, the behavior of the diffusion coefficient is readily determined as D_N should be roughly inversely proportional to $\tau(N)$.

The relative values of $\tau(52)$ and $\tau(53)$ are not self-evident just from inspection of the different forms the MEPs in Fig. 8 for $N = 52$ and $N = 53$, which we emphasize have the same $\delta E_{max} = \max_q \delta E(q) = 4\phi$. However, numerical integration of the master eqn (15) using Mathematica™ reveals that $\tau(52)/\tau(53)$ exceeds unity for all T corresponding to $D_{53}/D_{52} > 1$ consistent with KMC results. See the ESI.† This analysis is not quantitative predicting $D_{53}/D_{52} \approx 1.8$ at 700 K *versus* 1.1 from KMC simulation. However, we note that our master equation treatment has still not incorporated the influence of "excited state" configurations above the MEP and associated configurational entropy which can significantly change predictions.[33]

Finally, recall that in Fig. 6, results were presented for $\delta E(q)$ *versus* q for a broad range of "ideal" closed-shell TP sizes, N, showing that the MEP analysis predicts an increase in E_{eff} roughly linearly with NC height (or width). It is not viable to perform accurate KMC simulation analysis of D_N for such a broad the range of N. However, Fig. 9 compares KMC, MEP and refined-MF predictions for E_{eff} for closed-shell TP sizes where KMC results are available providing evidence that the MEP analysis captures the key features of the variation of the effective barrier, $E_{eff}(N)$, with N. The increase in $E_{eff}(N)$ with N is evident from KMC analysis for smaller N similar to the MEP predictions, and in contrast to the refined-MF predictions. The feature that the variation of KMC values for $E_{eff}(N)$ with N is somewhat irregular for these closed-shell TP reflects the feature that not all closed-shell TPs are equally stable (relative to other similar sized NCs). For example, the "ideal" closed-shell TP sizes $N = 13, 50, 126, \ldots$ (as analyzed in Fig. 6) which match the continuum Winterbottom shape are particularly stable, and the corresponding E_{eff} are relatively high compared to other non-ideal TP with comparable sizes. Again, accurate KMC values for E_{eff} tend to be somewhat below MEP predictions, presumably due to the neglect of the effects of configurational entropy, the contribution of which could increase for larger NC sizes.[33]

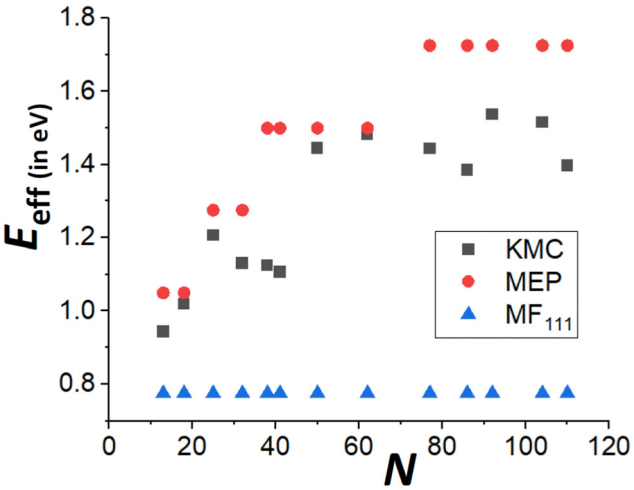

Fig. 9 Comparison of E_{eff} for closed-shell Ag TP from KMC simulation, beyond-MF MEP analysis, and refined-MF analysis for a ranges of sizes, N.

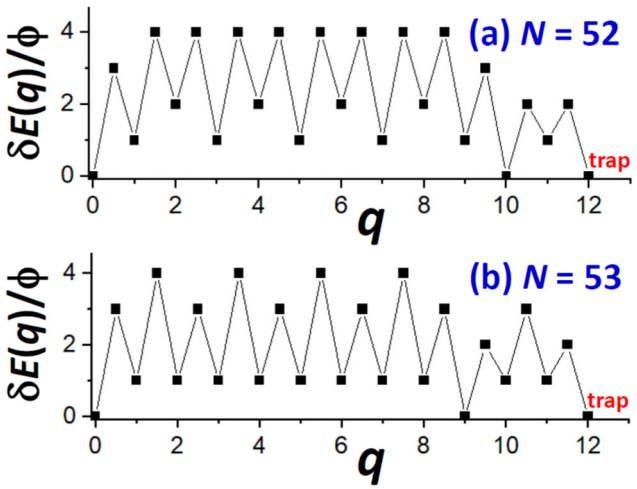

Fig. 8 Comparison of MEP $\delta E(q)$ *versus* q for: (a) $N = 52$; and (b) $N = 53$.

Conclusions

This study provided a critical assessment of mean-field (MF) treatments and their refinements for the size-dependent diffusivity, D_N, for the case of {100} epitaxially supported 3D fcc metal NCs of N atoms. Essentially exact behavior for D_N *versus* N for a realistic stochastic model for the above class of systems is obtained from KMC simulation for strong adhesion to the substrate where the large-size equilibrium Winterbottom shape of the supported NC is a truncated pyramid. MF treatments regard NC diffusion as being mediated by independent random hopping of surface atoms. As our specific focus was on faceted NCs, the traditional MF treatment was refined to account for the feature that the density of mobile surface atoms (which is primarily determined by their formation energy), as well as their hop rates, differ on distinct facets and at the base of the

NC. For our specific stochastic model, we performed an exact calculation of the formation energy and associated adatom density for a range of sizes N. This analysis accounted for the atomistic details of NC structure and energetics, *e.g.*, the existence of particularly stable close-shell sizes, $N = N_{cs}$. This refined MF treatment was able to capture the feature that D_N determined accurately from KMC simulation exhibited local minima for $N = N_{cs}$, but substantially higher and similar values for $N = N_{cs} + 2$ or $N = N_{cs} + 3$ (although the former are slightly higher in the MF treatment *versus* the latter for KMC). However, this refined-MF treatment did fail in that it predicted local maxima in D_N for $N = N_{cs} + 1$.

More significantly, our analysis also revealed more fundamental shortcomings of even refined MF-type treatments. These shortcomings derive from the feature that diffusion of faceted NCs is actually not mediated by independent random hopping of surface atoms, as assumed in MF formulations. Instead, NC diffusion is mediated by a cooperative multi-step process involving disassembling outer layers of atoms on side facets, transferring those atoms to another side facet on which a new outer layer is formed. The effective barrier for this multi-step nucleation type process is typically far higher than the barrier associated with the MF formulation which just corresponds to that for the single-atom hopping process of forming a single mobile surface adatom. The actual effective barrier increases strongly with NC size in marked contrast to the effective barrier in MF type treatments which converges to a finite value in the limit of large NC size. The feature that the effective MF barrier is well below the actual barrier also accounts for the feature that MF predictions for D_N are well above the actual values (a feature which is only partly ameliorated by including the effect of an additional Ehrlich-Schwoebel barrier in the MF treatment).

Finally, we note that our beyond-MF picture for diffusion of supported NCs should apply more generally for faceted NCs. Diffusion of all such NCs requires disassembly of one of more facets on one side of the NC and reassembly on another side. Of course, the process and its analysis is significantly more complicated for weak adhesion where the Winterbottom shape of the supported NC has overhanging facets (see Fig. 1), and it is clear that multiple facets must be disassembled and reassembled to shift the NC across the substrate and recover its initial structure. On a separate topic, we should note that for any faceted NC, one anticipates that as temperature increases, MF-type behavior will be recovered (implying a strong reduction in the oscillatory variation of D_N with N between consecutive close-shell sizes observed for lower T).[22] In this context, it should be noted that the roughening transition for small faceted metal NCs generally occurs well below the bulk roughening temperature promoting the recover of MF-type behavior.

Author contributions

K. C. L. and J. W. E. developed the stochastic model and performed related analysis of energetics and beyond-mean-field analysis of NC diffusion. K. C. L. performed KMC simulations for the stochastic model. J. W. E. developed and performed the refined mean-field analysis. K. C. L., C. T. C., and J. W. E. were involved in discussions of this work. J. W. E. wrote an initial draft of the manuscript, and C. T. C. and J. W. E. revised that draft.

Conflicts of interest

The authors have no conflict of interest.

Acknowledgements

J. W. E thanks Dr Da-Jiang Liu for discussions on this work. K. C. L. and J. W. E. were supported for this work by the US Department of Energy, Office of Science, Basic Energy Sciences, Division of Chemical Sciences, Geosciences, and Biological Sciences through the Computational and Theoretical Chemistry project at Ames National Laboratory (AL). AL is operated by Iowa State University under contract no. DE-AC02-07CH11358. C. T. C. acknowledges the US Department of Energy, Office of Science, Basic Energy Sciences for support of this work under Grant Number DE-FG02-96ER14630.

References

1 L. Ratke and P. W. Voorhees, *Coarsening and Growth: Ostwald Ripening in Materials Processes*, Springer, Berlin, 2001.
2 M. Zinke-Allmang, L. C. Feldman and M. H. Grabow, *Surf. Sci. Rep.*, 1992, **16**, 377–463.
3 W. Ostwald, *Lehrbuch der Allgemeinen Chemie*, Leipzig, Germany, 1896, vol. 2, Part 1.
4 I. M. Lifshitz and V. V. Slyozov, *J. Phys. Chem. Solids*, 1961, **19**, 35–50.
5 C. Z. Wagner, *Electrochem*, 1961, **65**, 581–591.
6 P. Wynblatt and N. A. Gjostein, *Prog. Solid State Chem.*, 1975, **9**, 21–58.
7 J. A. Farmer and C. T. Campbell, *Science*, 2010, **329**, 933–936.
8 S. R. Challa, A. T. Delariva, T. W. Hansen, S. Helveg, J. Sehested, P. L. Hansen, F. Garzon and A. K. Datye, *J. Am. Chem. Soc.*, 2011, **133**, 20672–20675.
9 T. W. Hansen, A. T. DeLaRiva, S. R. Challa and A. K. Datye, *Acc. Chem. Res.*, 2013, **46**, 1720–1730.
10 F. F. Tao and P. A. Crozier, Atomic-Scale Observations of Catalyst Structures under Reaction Conditions and during Catalysis, *Chem. Rev.*, 2016, **116**, 3487–3539.
11 Y. Dai, P. Lu, Z. Cao, C. T. Campbell and Y. Xia, *Chem. Soc. Rev.*, 2018, **47**, 4314–4331.
12 K. C. Lai, Y. Han, P. Spurgeon, W. Huang, P. A. Thiel, D.-J. Liu and J. W. Evans, *Chem. Rev.*, 2019, **119**, 6670–6768.
13 M. Rahmati, M. S. Safdari, T. H. Fletcher, M. D. Argyle and C. H. Bartholomew, *Chem. Rev.*, 2020, **120**, 4455–4533.
14 S. L. Hu and W. X. Li, *Science*, 2021, **374**, 1360–1365.
15 E. Ruckenstein and B. Pulvermacher, *AIChE J.*, 1973, **19**, 356–364.

16 M. J. J. Jak, C. Konstapel, A. van Kreuningen, J. Verhoeven and J. W. M. Frenken, *Surf. Sci.*, 2000, **457**, 295–310.
17 M. J. J. Jak, C. Konstapel, A. van Kreuningen, J. Chrost, J. Verhoeven and J. W. M. Frenken, *Surf. Sci.*, 2001, **474**, 28–36.
18 S. C. Parker and C. T. Campbell, *Phys. Rev. B: Condens. Matter Mater. Phys.*, 2007, **75**, 035430.
19 S.-L. Hu and W.-X. Li, *Sci. China: Technol. Sci.*, 2019, **62**, 762–772.
20 P. N. Plessow and C. T. Campbell, *ACS Catal.*, 2022, **12**, 2302–2308.
21 E. E. Gruber, *J. Appl. Phys.*, 1967, **38**, 243–250.
22 K. C. Lai and J. W. Evans, *Nanoscale*, 2019, **11**, 17506–17516.
23 L. T. Roling, L. Li and F. Abild-Pedersen, *J. Phys. Chem. C*, 2017, **121**, 23002–23010.
24 J. W. Evans, P. A. Thiel and M. C. Bartelt, *Surf. Sci. Rep.*, 2006, **61**, 1–128.
25 P. A. Thiel, M. Shen, D.-J. Liu and J. W. Evans, *J. Phys. Chem. C*, 2009, **113**, 5047–5067.
26 C. R. Henry, *Prog. Surf. Sci.*, 2005, **80**, 92–116.
27 K. C. Lai and J. W. Evans, *Phys. Rev. Mater.*, 2019, **3**, 026001.
28 K. C. Lai, M. Chen, B. M. Williams, Y. Han, C.-K. Tsung, W. Huang and J. W. Evans, *ACS Nano*, 2020, **14**, 8551–8561.
29 N. Combe, P. Jensen and A. Pimpinelli, *Phys. Rev. Lett.*, 2000, **85**, 110–113.
30 T. H. Lim, D. N. McCarthy, S. C. Hendy, K. J. Stevens, S. A. Brown and R. D. Tilley, *ACS Nano*, 2009, **3**, 3809.
31 D. N. McCarthy and S. A. Brown, *Phys. Rev. B: Condens. Matter Mater. Phys.*, 2009, **80**, 064107.
32 L. Li, P. N. Plessow, M. Rieger, S. Sauer, R. S. Sanchez-Carrera, A. Schaefer and F. Abild-Pedersen, *J. Phys. Chem. C*, 2017, **121**, 4261–4269.
33 K. C. Lai, D.-J. Liu and J. W. Evans, *J. Chem. Phys.*, 2023, **158**, 104102.
34 K. C. Lai, J. W. Evans and D.-J. Liu, *J. Chem. Phys.*, 2017, **147**, 201101.
35 K. C. Lai, D.-J. Liu and J. W. Evans, *Phys. Rev. B*, 2017, **96**, 235406.